Upgraded metallurgical-grade silicon solar cells with efficiency above 20%

P. Zheng, F. E. Rougieux, C. Samundsett, Xinbo Yang, Yimao Wan, J. Degoulange, R. Einhaus, P. Rivat, and D. Macdonald

Citation: Appl. Phys. Lett. **108**, 122103 (2016);
View online: https://doi.org/10.1063/1.4944788
View Table of Contents: http://aip.scitation.org/toc/apl/108/12
Published by the American Institute of Physics

Upgraded metallurgical-grade silicon solar cells with efficiency above 20%

P. Zheng,[1] F. E. Rougieux,[1] C. Samundsett,[1] Xinbo Yang,[1] Yimao Wan,[1] J. Degoulange,[2] R. Einhaus,[2] P. Rivat,[3] and D. Macdonald[1]
[1]*Research School of Engineering, College of Engineering and Computer Science, The Australian National University, Canberra, Australian Capital Terrritory 2601, Australia*
[2]*Apollon Solar, 66 Cours Charlemagne, Lyon 69002, France*
[3]*FerroPem, 517 Avenue de la Boisse, Chambery Cedex 73025, France*

(Received 4 January 2016; accepted 13 March 2016; published online 22 March 2016)

We present solar cells fabricated with *n*-type Czochralski–silicon wafers grown with strongly compensated 100% upgraded metallurgical-grade feedstock, with efficiencies above 20%. The cells have a passivated boron-diffused front surface, and a rear locally phosphorus-diffused structure fabricated using an etch-back process. The local heavy phosphorus diffusion on the rear helps to maintain a high bulk lifetime in the substrates via phosphorus gettering, whilst also reducing recombination under the rear-side metal contacts. The independently measured results yield a peak efficiency of 20.9% for the best upgraded metallurgical-grade silicon cell and 21.9% for a control device made with electronic-grade float-zone silicon. The presence of boron-oxygen related defects in the cells is also investigated, and we confirm that these defects can be partially deactivated permanently by annealing under illumination. © *2016 AIP Publishing LLC*.
[http://dx.doi.org/10.1063/1.4944788]

Upgraded Metallurgical-Grade (UMG) silicon has raised interest as a low cost alternative material for high efficiency silicon solar cells.[1–7] UMG silicon feedstock is purified using a liquid phase purification process. As a result, it contains more impurities, especially shallow acceptors and donors (B, Al, and P), and the minority carrier lifetime is usually lower in the as-grown state. In addition, due to dopant compensation, the carrier mobility is reduced, and the presence of boron leads to the formation of the boron-oxygen (BO) defect, even in *n*-type compensated UMG silicon wafers.[8–10] Recent improvements in the UMG purification process have led to an improvement in feedstock quality. In this paper, we present a high efficiency (20.9%) silicon cell based on 100% solar-grade feedstock, using *n*-type Czochralski-grown (Cz) wafers.

With the advent of higher quality UMG material,[11] reported cell efficiencies using this material have improved significantly in the recent years. For *p*-type UMG silicon solar cells, in 2010, an efficiency of 17% was reported for multi-crystalline silicon (mc-Si) solar cells, with an average batch efficiency of 16.4%. An efficiency of 17.6% was also achieved for a *p*-type monocrystalline UMG silicon solar cell, with an average batch efficiency of 17.4% using the same process.[4] In 2011, comparable cell efficiencies were achieved for *p*-type mc-Si UMG solar cells and cells made with standard electronic-grade feedstock, of 18.35% and 18.45%, respectively.[5] By switching from *p*-type to *n*-type UMG, in 2012, 19% efficiency was achieved using 100% UMG Cz silicon with a heterojunction device.[6] This was then followed by a 19% *n*-type UMG Cz homojunction cell one year later.[7] Recently, Rougieux *et al.*[12] reported a 19.8% efficient Passivated Emitter Rear Totally diffused (PERT) cell using 100% UMG *n*-type Cz.

In this paper, we present an *n*-type Cz cell with an efficiency of 20.96% using 100% UMG feedstock, and describe the optimised device design and the impact of boron-oxygen-related defects on device performance.

In this study, we have used two different types of *n*-type monocrystalline silicon wafers. The first type was from a 9.5 kg ingot with a diameter of 6 inch, grown with 100% UMG silicon feedstock without adding electronic grade (EG) polysilicon feedstock using the Czochralski process. The second type was from a Float-Zone (FZ) grown ingot using standard EG silicon feedstock. The UMG feedstock was produced by FerroPem in the framework of the PHOTOSIL project. The wafers had resistivities of 4 Ω cm (solidified fraction $f_s = 20\%$) for the UMG material and 1 Ω cm for the EG wafers. The doping density of both phosphorus and boron was measured by Secondary Ion Mass Spectrometry (SIMS) analysis, showing that the UMG wafers had a boron concentration of $[B] = 1.27 \times 10^{16}\,cm^{-3}$ and a phosphorus concentration of $[P] = 1.42 \times 10^{16}\,cm^{-3}$, which results in a net doping of $n_0 = 1.4 \times 10^{15}\,cm^{-3}$. The oxygen and carbon concentrations of the UMG wafers were $[O] = 6.6 \times 10^{17}\,cm^{-3}$ and $[C] = 6.1 \times 10^{16}\,cm^{-3}$, respectively. The concentrations of metallic impurities were below the detection limit of Inductively Coupled Plasma Mass Spectrometry (ICPMS). The EG wafers were non-compensated and had a majority carrier concentration of $n_0 = [P] = 4.8 \times 10^{15}\,cm^{-3}$, as determined by the dark conductance measurements.

The cell structure used in this study is a Passivated Emitter Rear Locally diffused (PERL) solar cell structure,[13] specially adapted to maintain a high carrier lifetime in the UMG material, and is represented in Figure 1. The cells were $2 \times 2\,cm^2$ in size. The front surface was random pyramid textured using tetramethylammonium hydroxide (TMAH) and isopropyl alcohol (IPA) solution. The emitter was formed by full-area boron diffusion with a sheet resistance of approximately 120 Ω/□ at 940 °C of 17 min deposition in an atmosphere of mixture of O_2, N_2, and BBr_3. The rear localized diffusions were 75 μm diameter dots with a hexagonal pitch of 300 μm, which was formed by a full-area phosphorous diffusion and etch back in TMAH solution. The sheet resistance

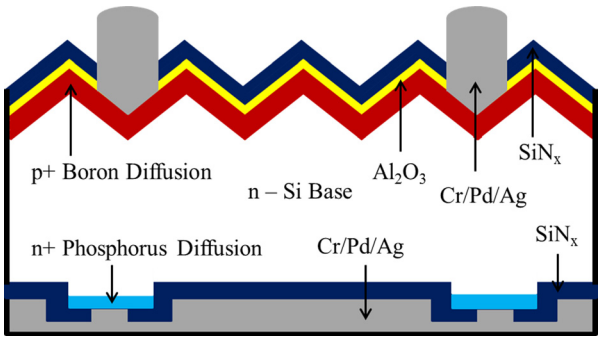

FIG. 1. Schematic diagram of *n*-type UMG silicon solar cell with full front boron diffusion and rear etch-back localized phosphorus diffusion, Al_2O_3/SiN_x stack at the front and SiN_x at the rear side and with Cr/Pd/Ag stacks for both the front and rear metallization.

was approximately 70 Ω/□ at 790 °C of 25 min deposition in an atmosphere of mixture of O_2, N_2, and $POCl_3$. The front surface passivation layer was an Al_2O_3/SiN_x stack, and the rear passivation layer was a single SiN_x film. The Al_2O_3 film was deposited by Atomic Layer Deposition (ALD) at 175 °C and then activated at 400 °C and SiN_x by Plasma-Enhanced Chemical Vapour Deposition (PECVD) at 400 °C. Front and rear contact areas were defined by photolithography followed by the thermal evaporation of Cr/Pd/Ag stacks with subsequent Ag electroplating of the front fingers to increase the finger thickness. The contacts were sintered at 350 °C for 30 min in forming gas (FGA). The front finger contact openings were 10 μm wide prior to plating, with a spacing of 1.3 mm. The rear contact openings were 30 μm in diameter and had the same pitch as the localized diffusion.

In order to measure the recombination parameter J_0 of the front textured boron diffusion, we used 100 Ω cm *n*-type control wafers. To measure the J_0 for the un-diffused rear side passivated with SiN_x, we used sister wafers to those used for cells. Dark IV measurements were performed using a Keithley 2400 source meter to extract the shunt resistance (R_{sh}).[14] The contact resistivity (ρ_c) was measured using Transfer Length Method (TLM) measurements.[15] Suns-V_{oc} measurements[16] were performed to evaluate the lumped series resistance (R_s) at the maximum power point.[17]

In order to investigate the impact of high temperature processing (boron and phosphorus diffusion) on the minority carrier lifetime of the UMG wafers, we used sister wafers ($f_s = 23\%$) to the cell wafers ($f_s = 20\%$). The FZ EG control wafers from the same ingot as the EG cell of resistivity 1 Ω cm were also included. The samples were TMAH etched after processing to remove the boron and phosphorus diffusions, and then passivated by PECVD SiN_x. The bulk lifetimes of both the samples before and after processing are shown in Figure 2. The UMG sample had an initial as-cut lifetime above 1 ms, while the EG FZ control wafer had an initial as-cut lifetime of several milliseconds. The samples then underwent boron diffusion. The bulk lifetimes degraded to around 100 μs and 200 μs after boron diffusion for the UMG and FZ wafers, respectively. The reduction of the bulk lifetime after boron diffusion in both the UMG and FZ controls indicates some process contamination. In addition to the process contamination, the lower lifetime in the UMG wafers indicates the additional presence of residual impurities in these wafers that are activated during the boron diffusion.

After the boron diffusion, the samples were then subjected to phosphorus diffusion, as required to allow ohmic contact to the rear side of the devices. It can be seen from Figure 2 that the phosphorus diffusion also recovers the bulk lifetime to above 500 μs for both the wafer types, due to gettering of mobile impurities introduced during the boron diffusion. Note that the diffusion is optimized for cell front diffusion and not for gettering; hence recovery of the lifetime is only partial in these wafers. Therefore, a process with phosphorus gettering after boron diffusion is important for the UMG wafers. To maintain a high bulk lifetime in the UMG cells, relatively heavy and full area phosphorus diffusion was chosen for the cell process. However, a heavy phosphorus diffusion will significantly increase recombination on the non-metallised portion of the rear side, for a device with a full rear-side diffusion, such as the Passivated Emitter and Rear Totally diffused (PERT) cells we have reported previously on similar material.[12] Therefore, a PERL structure was selected to minimise the area of the diffused regions to achieve high efficiency UMG solar cells. Crucially, the

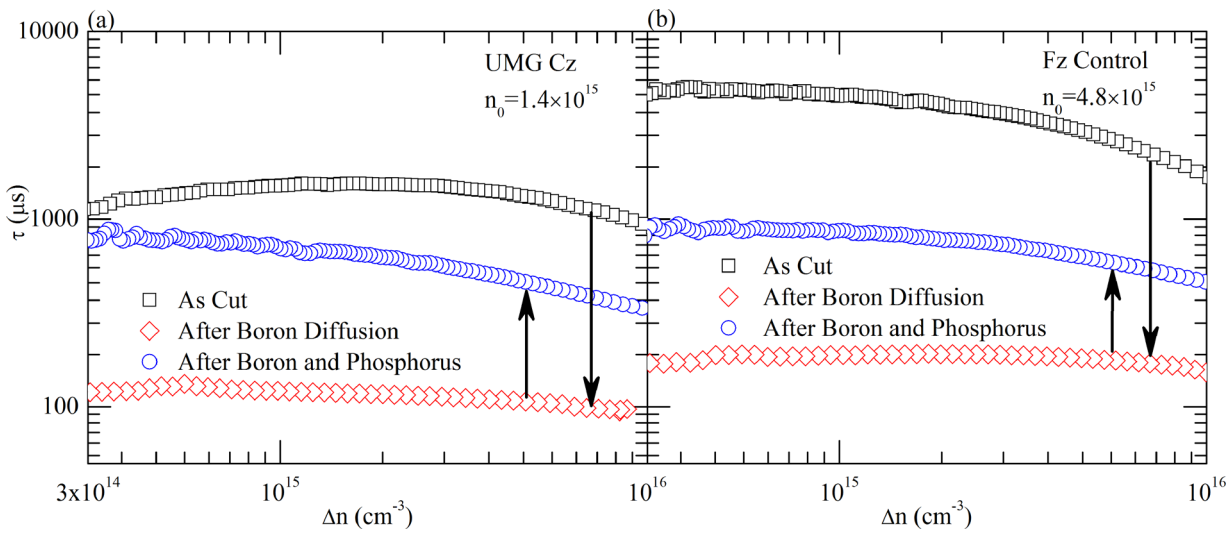

FIG. 2. Injection dependent minority carrier bulk lifetime (a) *n*-type FZ 1 Ω cm control wafer and (b) *n*-type UMG Cz silicon wafers in the as-cut state, after boron diffusion, and after both boron and phosphorus diffusions.

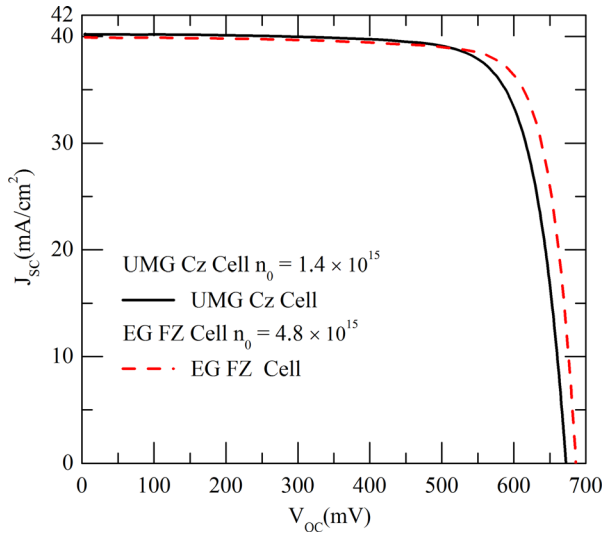

FIG. 3. Independent illuminated IV measurements of the best *n*-type UMG Cz and EG FZ cells, measured at Fraunhofer CalLab.

TABLE I. Dopant concentration and type, net doping n_0, and thickness W of the UMG Cz and EG FZ cells.

Cell	[P] (cm^{-3})	[B] (cm^{-3})	n_0 (cm^{-3})	W (μm)
UMG Cz	1.42×10^{16}	1.27×10^{16}	1.4×10^{15}	150
EG FZ	4.8×10^{15}	…	4.8×10^{15}	170

localization of the diffusion at the rear side is achieved by an-etch back process, instead of being diffused locally into the contact area, in order to maintain a full-area gettering effect. In addition, the heavy local phosphorus diffusion has the benefit of reducing recombination under the metal contacts, in comparison to the lighter diffusions usually required for an efficient PERT device.

Independent measurements of the illuminated current-voltage characteristics at Fraunhofer CalLab confirm an efficiency of 20.96% and 21.91% for the best *n*-type UMG Cz cell and the best EG FZ cell, respectively. The IV curves are plotted in Figure 3. The thickness, dopant concentrations, and net doping n_0 ($n_0 = [P] - [B]$ for the UMG material) of the cells are shown in Table I. Details of the extracted cell parameters are shown in Table II. Device parameters measured on the control wafers are reported in Table III.

The External Quantum Efficiency (EQE) and reflectance measurements for the best cells are shown in Figure 4. These reveal a slightly higher EQE for the UMG cell in the wavelength range from 300 to 900 nm, especially in the range from 300 nm to 600 nm. This difference results from a slight difference in the random texturing at the front surface and minor variations in the thickness of SiN_x capping layer on the front surface. To confirm this, the reflectance of both the cells was measured. Figure 4 shows the reflectance measurements for

TABLE III. Cell parameters measured on the control wafers for both front and rear sides of the cells.

Side	Properties	Value
Front	Sheet resistance	120 Ω/□
	$R_{contact}$	0.06 mΩ cm^2
	$J_{0\text{-}passivated}$	45 fA/cm^2
Rear	Sheet resistance	70 Ω/□
	$R_{contact}$	0.024 mΩ cm^2
	$J_{0\text{-}passivated}$	3 fA/cm^2

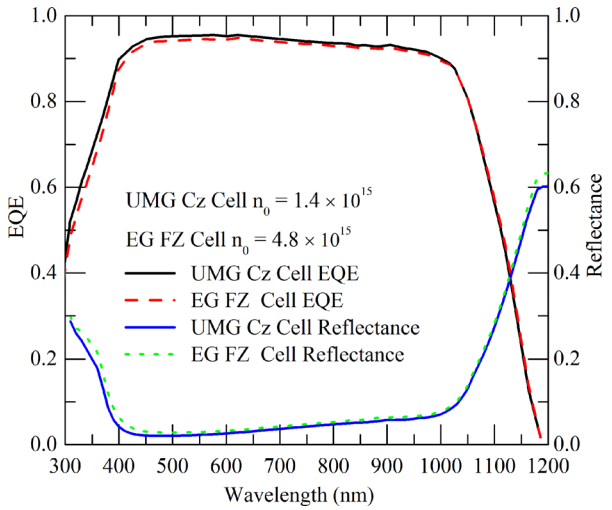

FIG. 4. EQE measurement of the best *n*-type UMG Cz and EG FZ cells (measured at Fraunhofer CalLab) also shown is the Reflectance for both cells.

both the UMG and FZ cells. It confirms that the reflectance for FZ cell is slightly higher than that for UMG cell in the range from 300 nm up to 900 nm. Of particular note is the fact that the UMG and FZ cells are almost identical in their EQE in the long wavelength range between 900 nm and 1200 nm. This indicates that the minority carrier diffusion length is significantly larger than the wafer thickness for both the UMG and FZ cells, despite the expected impact of the strong dopant compensation on the carrier mobilities in the UMG material. Based on the carrier lifetimes in Figure 2, the minority carrier diffusion lengths for the UMG and FZ cells are estimated to be 695 μm and 1018 μm, with the minority carrier mobilities estimated using Schindler's model[18] of 372 cm^2 V^{-1} s^{-1} and 399 cm^2 V^{-1} s^{-1}. These diffusion lengths are more than three times the device thickness, resulting in almost complete carrier collection at the front junction.

The impact of the BO related-defect has been extensively studied in *p*-type boron doped and compensated silicon, as well as in *n*-type compensated silicon for several years.[8,10,19,20] Recently, the focus has moved to the permanent deactivation of the BO defects[21–25] by annealing under

TABLE II. Extracted parameters from the illuminated IV, dark IV, and Suns-V_{oc} characteristics.

Cell	J_{sc} (mA cm^{-2})	V_{oc} (mV)	J_{mpp} (mA cm^{-2})	V_{mpp} (mV)	FF (%)	η (%)	R_{sh} (Ω cm^2)	$R_{s,mpp}$ (Ω cm^2)	PFF
UMG Cz	40.23	672.6	37.03	566.1	77.5	20.96	8000	0.77	82.2
EG FZ	39.89	686.2	37.03	591.7	80.1	21.91	5000	0.35	81.5

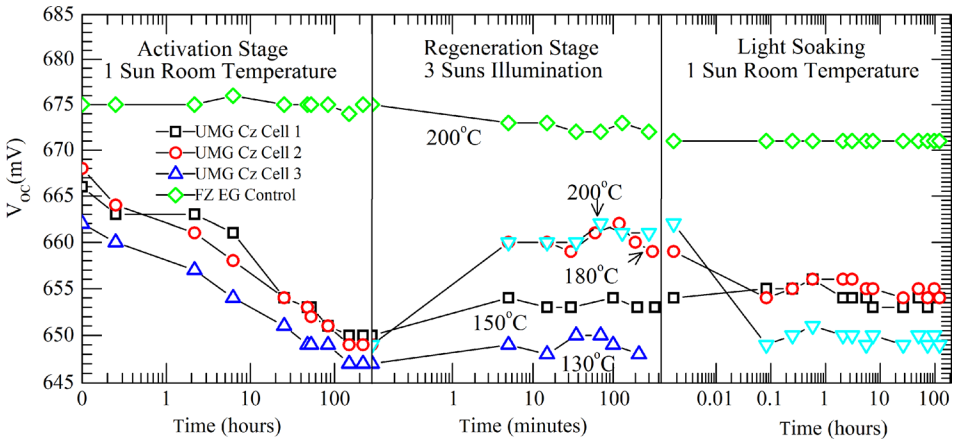

FIG. 5. The V_{oc} evolution due to the boron-oxygen related defect of 3 investigated UMG Cz Cells through 3 different stages: an Activation stage, a Regeneration stage, and a Light Soaking stage (stability test).

illumination or bias. In this experiment, the *n*-type PERL UMG solar cells are used to investigate the impact of the BO defect at the cell level. The V_{oc} evolution of the cells is shown in Figure 5. For the defect activation stage, the V_{oc} of the UMG cells degraded by approximately 17 mV over a 200 h illumination at an intensity of 1 sun, while the FZ control cell did not experience any degradation, as expected. The regeneration was then performed at four different temperatures ranging from 130 °C to 200 °C under an illumination intensity of 3 suns. The V_{oc} improvements increased with the increasing temperature. The cell annealed at 130 °C (Cell 3) did not see significant improvement. However, Cell 3 showed a fast improvement during subsequent annealing at 200 °C. The same control cell was used for all the processes and only experienced slight degradation during the final 200 °C annealing. The stability of the regenerated cells was then tested under 1 sun light intensity over 200 h. Cell 3, which was regenerated at 200 C, showed a fast degradation back to the level of the degraded cells under illumination. Cell 1, which was regenerated at 150 °C, did not show any degradation and remained at approximately 655 mV. Cell 2 degraded slightly and saturated at the same level as Cell 1.

Munzer[21] and Herguth *et al.*[22] reported regeneration of the BO defect in *p*-type silicon solar cells at 50 to 75 °C, and showed that the regenerated cells had similar V_{oc} and efficiencies as the cells before degradation. The cells were stable under illumination of 1 sun intensity over 200 h. However, from Figure 5, it can be seen that the V_{oc} of the regenerated cells cannot be recovered to the initial value. Niewelt *et al.*[23] used *n*-type compensated wafers with similar oxygen, boron, and phosphorus concentrations for a regeneration experiment, and showed on lifetime structures that the regeneration cannot recover the bulk lifetime to the initial level with non-optimized curing conditions. The non-optimized temperature and the illumination intensity could therefore explain the partial recovery of V_{oc} in this study. The slight degradation of Cell 2 and complete degradation of Cell 3 during the stability test could also be related to the non-optimized curing conditions. As suggested by Wilking *et al.*,[24] when starting from a fully degraded state, the reactions creating the annealed state and permanently deactivated state of the BO defect are competing reactions. Their kinetics depends on the temperature. If the temperature is too high, the kinetics of the reaction creating the annealed state will be faster than the reaction producing the permanently deactivated state. Hence, most of the BO defect will transform into the annealed state rather than the permanently deactivated state. This is likely to be the reason that Cells 2 and 3 degraded during the final stability test. The reason for the much faster degradation rate of Cell 3 during the light soaking after permanent deactivation compared to the initial light soaking is still unclear. Various authors have proposed physical explanations of the regeneration process. Voronkov *et al.*[26] suggested that the regeneration process was due to the loss of interstitial boron to boron nano-precipitates during simultaneous annealing and illumination. Upon subsequent illumination, no interstitial boron is present and therefore no recombination active BO can form. Hallam *et al.*[25] and Munzer[21] proposed that the regeneration is caused by the hydrogenation of BO defects and controlled by the charge state of hydrogen, which is strongly related to the temperature and illumination intensity, as also proposed by Sun *et al.*[27]

In conclusion, we have presented silicon solar cells based on 100% UMG Cz wafers with efficiencies above 20%, and only slightly lower than the efficiencies achieved for control FZ EG cells fabricated using the same process. This shows that with an optimised fabrication process, the bulk lifetime and minority carrier diffusion length are not strongly limiting factors for UMG material to achieve high efficiency devices. In addition, we have shown that BO defects still affect the efficiency of *n*-type UMG Cz solar cells. However, they can be partially deactivated with annealing under illumination. With an optimized illumination intensity and temperature, a more complete deactivation of this defect should be possible.

This work was supported by the Australian Renewable Energy Agency (ARENA) through the Australian Center for Advanced Photovoltaics (ACAP), Project RND009, and their Postdoctoral Fellowships program. D.M. acknowledges the support from the Australian Research Council through the Future Fellowships program.

[1]N. Yuge, H. Baba, Y. Sakaguchi, K. Nishikawa, H. Terashima, and F. Aratani, Sol. Energy Mater. Sol. Cells **34**(1), 243 (1994).
[2]K. Ounadjela and A. Bloss, "New metallization technique for 6 MW pilot production of multicrystalline solar cells using upgraded metallurgical grade silicon," NREL Technical Report No. NREL/SR-520-48591, CaliSolar, Inc., Sunnyvale, 2010.
[3]D. Kohle, B. Raabe, S. Braun, S. Seren, and G. Hahn, "Upgraded metallurgical grade silicon solar cells: A detailed material analysis," in *Proceeding*

of the 24th European Photovoltaic Solar Energy Conference, Hamburg, Germany (2009), pp. 1758–1761.
[4]J. Kraiem, B. Drevet, F. Cocco, N. Enjalbert, S. Dubois, D. Camel, D. Grosset-Bourbange, D. Pelletier, T. Margaria, and R. Einhaus, "High performance solar cells made from 100% UMG silicon obtained via the PHOTOSIL process," in *Proceeding of the 35th IEEE Photovoltaic Specialists Conference (PVSC)* (2010), pp. 001427–001431.
[5]P. Engelhart, J. Wendt, A. Schulze, C. Klenke, A. Mohr, K. Petter, F. Stenzel, S. Hörnlein, M. Kauert, M. Junghänel, B. Barkenfelt, S. Schmidt, D. Rychtarik, M. Fischer, J. W. Müller, and P. Wawer, Energy Procedia **8**, 313 (2011).
[6]R. Einhaus, J. Kraiem, J. Degoulange, O. Nichiporuk, M. Forster, P. Papet, Y. Andrault, D. Grosset-Bourbange, and F. Cocco, "19% efficiency heterojunction solar cells on Cz wafers from non-blended upgraded metallurgical silicon," in *Proceeding of the 38th IEEE Photovoltaic Specialists Conference (PVSC)* (2012), pp. 003234–003237.
[7]Y. Schiele, S. Wilking, F. Book, T. Wiedenmann, and G. Hahn, Energy Procedia **38**, 459 (2013).
[8]T. Schutz-Kuchly, J. Veirman, S. Dubois, and D. R. Heslinga, Appl. Phys. Lett. **96**(9), 093505 (2010).
[9]F. E. Rougieux, M. Forster, D. Macdonald, A. Cuevas, B. Lim, and J. Schmidt, IEEE J. Photovoltaics **1**(1), 54 (2011).
[10]F. E. Rougieux, B. Lim, J. Schmidt, M. Forster, D. Macdonald, and A. Cuevas, J. Appl. Phys. **110**(6), 063708 (2011).
[11]M. Forster, E. Fourmond, R. Einhaus, H. Lauvray, J. Kraiem, and M. Lemiti, Phys. Status Solidi C **8**(3), 678 (2011).
[12]F. Rougieux, C. Samundsett, K. C. Fong, A. Fell, P. Zheng, D. Macdonald, J. Degoulange, R. Einhaus, and M. Forster, Prog. Photovoltaics: Res. Appl. (to be published).
[13]M. A. Green, *Silicon Solar Cells: Advanced Principles and Practice* (Centre for Photovoltaic Devices and Systems, Sydney, Australia, 1995), pp. 219–220.
[14]I. Martil and G. Gonzalez Diaz, Eur. J. Phys. **13**(4), 193 (1992).
[15]D. L. Meier and D. K. Schroder, IEEE Trans. Electron Devices **31**(5), 647 (1984).
[16]R. A. Sinton and A. Cuevas, "A quasi-steady-state open-circuit voltage method for solar cell characterization," in *Proceeding of the 16th European Photovoltaic Solar Energy Conference, Hamburg, Germany* (2000), pp. 1152–1155.
[17]D. Pysch, A. Mette, and S. W. Glunz, Sol. Energy Mater. Sol. Cells **91**(18), 1698 (2007).
[18]F. Schindler, M. C. Schubert, A. Kimmerle, J. Broisch, S. Rein, W. Kwapil, and W. Warta, Sol. Energy Mater. and Sol. Cells **106**(0), 31 (2012).
[19]K. Bothe and J. Schmidt, J. Appl. Phys. **99**(1), 013701 (2006).
[20]D. Macdonald, F. Rougieux, A. Cuevas, B. Lim, J. Schmidt, M. Di Sabatino, and L. J. Geerligs, J. Appl. Phys. **105**(9), 093704 (2009).
[21]K. A. Münzer, "Hydrogenated silicon nitride for regeneration of light induced degradation," in *Proceeding of the 24th European Photovoltaic Solar Energy Conference Hamburg, Germany* (2009), pp. 1558–1561.
[22]A. Herguth, G. Schubert, M. Kaes, and G. Hahn, "A new approach to prevent the negative impact of the metastable defect in boron doped cz silicon solar cells," in C*onference Record of the 2006 IEEE 4th World Conference on Photovoltaic Energy Conversion* (2006), pp. 940–943.
[23]T. Niewelt, J. Broisch, J. Schön, J. Haunschild, S. Rein, W. Warta, and M. C. Schubert, Energy Procedia **77**, 626 (2015).
[24]S. Wilking, M. Forster, A. Herguth, and G. Hahn, Sol. Energy Mater. Sol. Cells **142**, 87 (2015).
[25]B. J. Hallam, S. R. Wenham, P. G. Hamer, M. D. Abbott, A. Sugianto, C. E. Chan, A. M. Wenham, M. G. Eadie, and G. Xu, Energy Procedia **38**, 561 (2013).
[26]V. V. Voronkov, R. Falster, B. Lim, and J. Schmidt, J. Appl. Phys. **112**(11), 113717 (2012).
[27]C. Sun, F. E. Rougieux, and D. Macdonald, J. Appl. Phys. **117**(4), 045702 (2015).